SUPPLEMENTAL MATERIAL

Supplemental Methods and Results

Data S1. Alternative Potential-Based Inverse Methods

We assessed four different potential-based inverse methods in the reconstruction of repolarization using the torso tank data. These included different combinations of two numerical methods to define the relationship between the heart and the torso (the method of fundamental solutions[23] and the boundary element method[24]), two methods to regularize the inverse problem (zero-order and second-order Tikhonov[25]), and two methods to determine the regularization parameter lambda, (the L-curve method[26] and the CRESO method[27]). The combinations are as follows:

1. The method of fundamental solutions with zero-order Tikhonov regularization and the CRESO method (MFS-TIKH0-CRESO) – the method used in the main manuscript.
2. The method of fundamental solutions with zero-order Tikhonov regularization and the L-curve method (MFS-TIKH0-Lcurve).
3. The boundary element method with zero-order Tikhonov regularization and the CRESO method (BEM-TIKH0-CRESO).
4. The boundary element method with second-order Tikhonov regularization and the CRESO method (BEM-TIKH2-CRESO) – the method used in previous studies for repolarization[3-5]).

Repolarization times (RT) were defined from recorded and ECGI-reconstructed electrograms as the time of maximum upslope of the T-wave, and the repolarization gradients (ΔRT) as the difference in RT between two adjacent electrodes divided by the distance between them.

Inverse reconstructions were compared to ground truth recorded electrograms using methods described in the main article. The lambda values computed by each method were also compared. Statistical analysis was conducted using GraphPad Prism 7.04. For each metric, the significance of differences was tested using a one-way ANOVA with $p<0.05$ defined as significant.

The MFS-Tikh0-CRESO method reconstructed T-waves, RTs and ΔRT better than most other methods tested (Figures S1 and S2 and Table S1). However, the absolute improvement in correlation and error metrics were minimal.

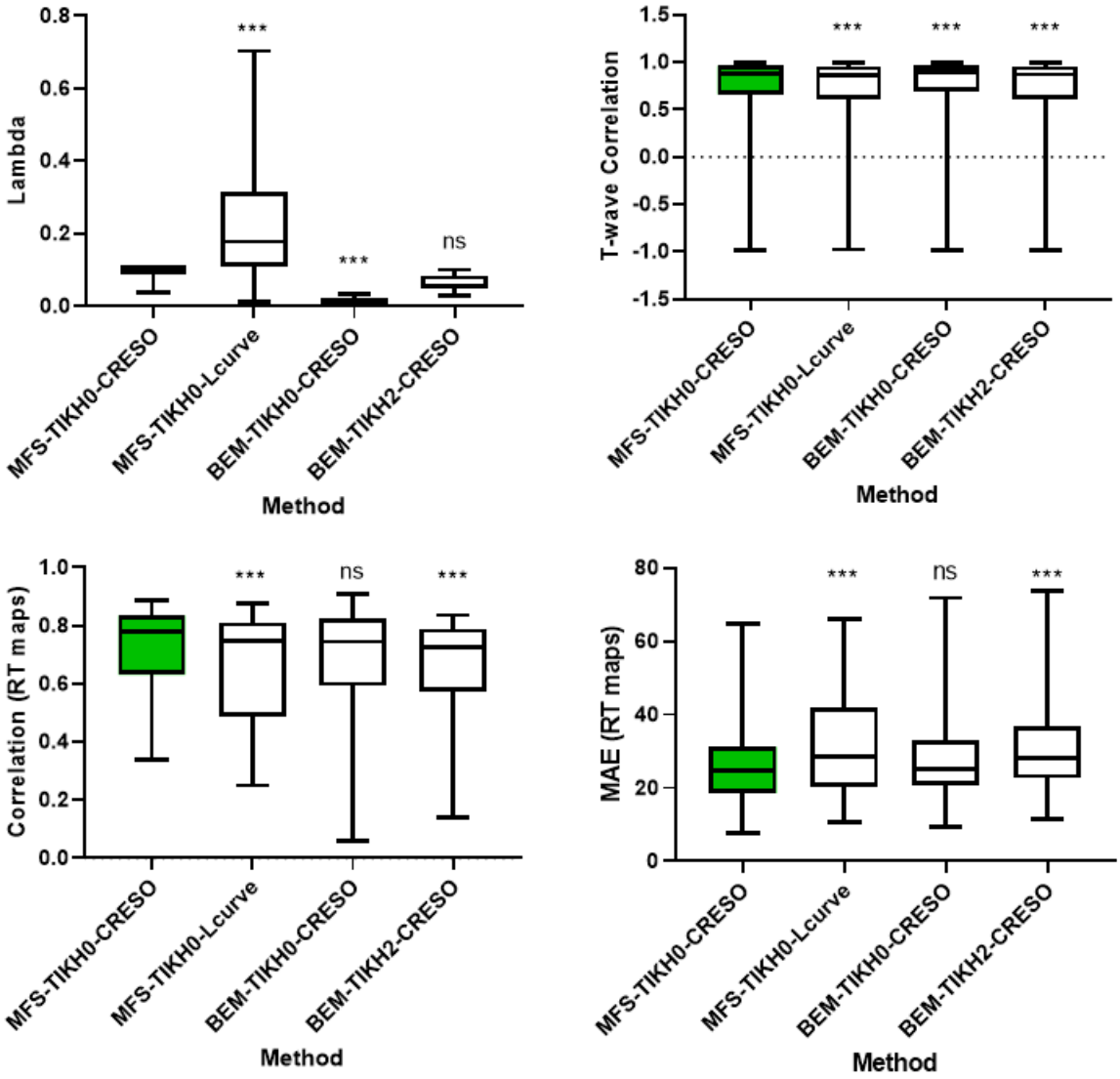

Figure S1.1: *Boxplots of the lambda used for regularization (top left), correlation of the T-wave (top right), correlation of RT maps (bottom left) and MAE of RT maps (bottom right) between recorded and reconstructed epicardial electrograms using 4 different inverse methods. Probabilities that distributions are significantly different to MFS-TIKH0-CRESO: *** $p \leq 0.0001$ and ns $p > 0.05$.*

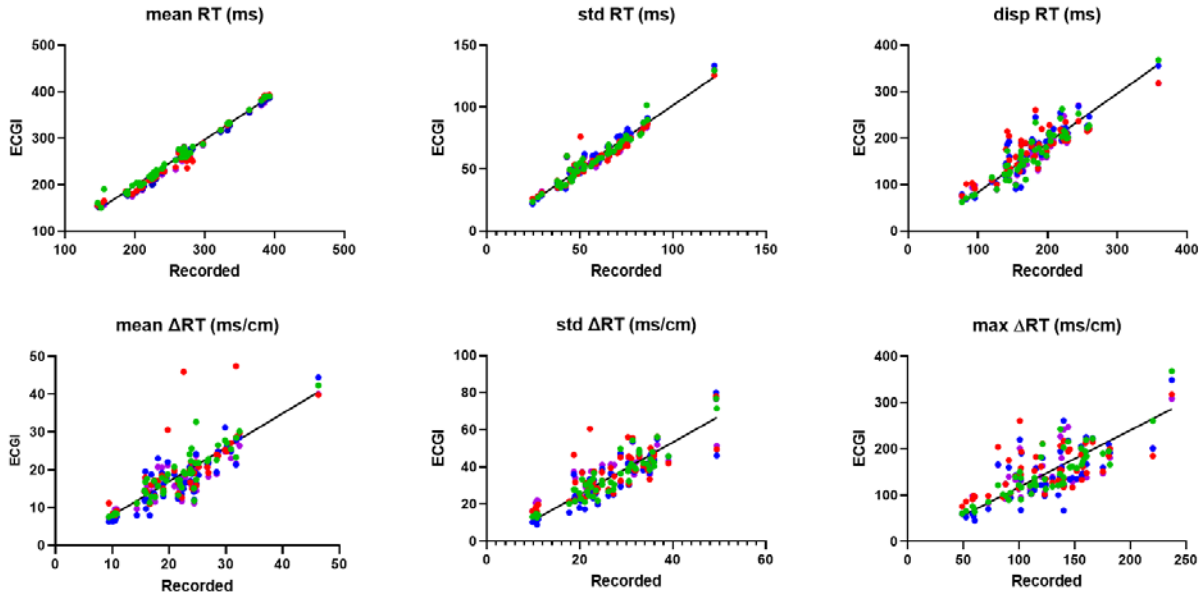

Figure S1.2: *Linear regression analysis between recorded and reconstructed RT (top line) and ΔRT distribution statistics using MFS-Tikh0-CRESO (green), MFS-Tikh0-Lcurve (red), BEM-Tikh0-CRESO (blue), and BEM-Tikh2-CRESO (purple). The linear regression (black line) is for MFS-Tikh0-CRESO. There was no significant difference between the slope nor the intercept for any method (p>0.05).*

		MFS-TIKH0-CRESO	MFS-TIKH0-L-CURVE	BEM-TIKH0-CRESO	BEM-TIKH2-CRESO
MEAN RT	R^2	0,98	0,98	0,99	0,98
	Sy.x	8,42	10,24	7,96	8,29
STD RT	R^2	0,95	0,91	0,96	0,95
	Sy.x	4,57	5,59	4,34	4,32
DISP RT	R^2	0,86	0,72	0,81	0,78
	Sy.x	21,79	25,84	25,61	24,49
MEAN ΔRT	R^2	0,80	0,54	0,76	0,74
	Sy.x	3,12	5,69	3,51	3,06
STD ΔRT	R^2	0,85	0,59	0,75	0,70
	Sy.x	5,29	8,20	6,77	6,46
MAX ΔRT	R^2	0,74	0,39	0,53	0,50
	Sy.x	29,66	38,66	41,51	36,06

Table S1. Linear regression R2 and $SS_{yy.xx}$ between recorded and reconstructed RT and ΔRT distribution statistics using the 4 different inverse methods.

Data S2. Spatial variability in accuracy

Spatial maps of T-wave CC and RT Abs Error demonstrated the ECGI reconstructions were more accurate within the early and late repolarization regions than at the gradient border (Figure S2.1).

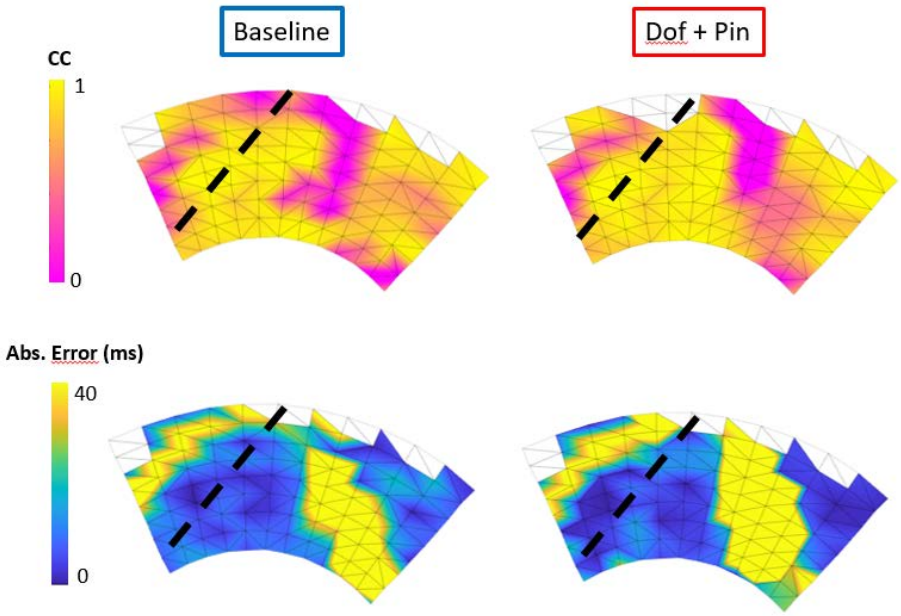

Figure S2.1: *Spatial maps of CC between recorded and reconstructed T-waves (top) as well as absolute error in RT (bottom) for the same case as Figure 2 at baseline (blue) and with combined dofetilide and pinacidil perfusion (red).*

To see if this occurred across all data sets, we compared each metric between regions with monophasic T-waves (early/late regions) and biphasic T-waves (regions of gradient). To separate monophasic and biphasic T-wave waveforms, the integral over the T-wave for each electrode was calculated:

$$\frac{\int_{Tonset}^{Toffset} \frac{V_i}{\max(V_i) - \min(V_i)}\, dt}{Toffset - Tonset}$$

Where the timing of $Tonset$ and $Toffset$ were defined manually, and V_i is the sock recorded potential at electrode i. Potentials were normalized to by the amplitude over the entire QRST to compensate for amplitude variations between electrodes. Postive T-waves (early regions) were defined when the integral was > 0.2, Negative T-waves (late regions) for integrals of < -0.2 and the remaining electrodes were defined as Biphasic.

Statistical analysis was conducted using GraphPad Prism 7.04. For each metric, the significance of differences was tested using a one-way ANOVA with $p<0.05$ defined as significant. Results are presented in Figure 2.2.

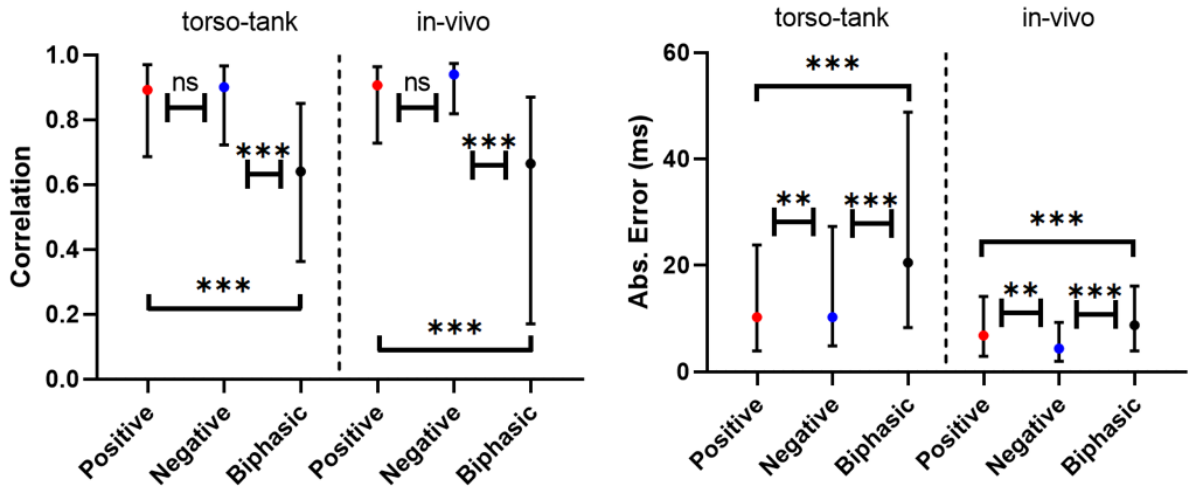

Figure S2.2: *Correlation between recorded and reconstructed T-waves (left) and absolute error in RT (right) for torso tank and in-vivo data. Values have been categorized by the positive monophasic (early recovery), negative monophasic (late recovery), or biphasic morphology of the T-wave. Probabilities that distributions are significantly different: *** $p\leq0.0001$, ** $p\leq0.01$, and ns $p>0.05$.*

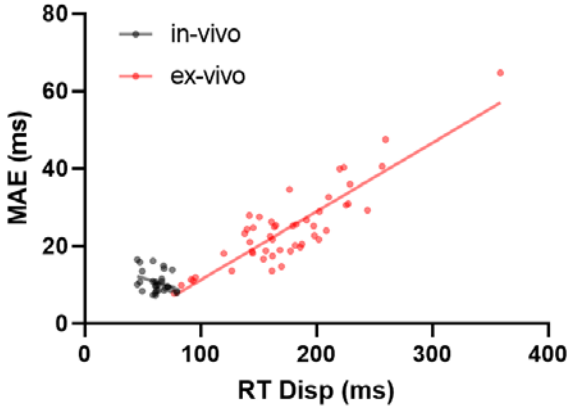

Figure S2.3: *Linear relationship between the MAE (between ECGI and recorded recovery times) and the total RT dispersion as recorded on the sock. One curve does not adequately fit both in-vivo (black) and ex-vivo torso tank (red) data ($p=0.002$). For ex-vivo data, $R^2 = 0.76$ and Sy.x. = 5.1 ms while for in-vivo data $R^2 = 0.10$ and Sy.x. = 2.7 ms.*

Figure S2.3 Demonstrates the linear relationship between the total RT dispersion and the MAE between ECGI and recorded recovery times for *in-vivo* and *ex-vivo* data. At low dispersion (no repolarization abnormalities), MAE is similar between *ex-vivo* and *in-vivo* data sets. At high dispersion (large repolarization abnormalities present), MAE increases for *ex-vivo* data. This increase is due to the steeper gradients in the transition zones and their spatial shift with ECGI, resulting in higher errors in RT times in the transition zone that, increases the overall mean absolute error.

Data S3. Beat-to-Beat Variability

Periodic beat-to-beat variation in the amplitude or shape of the T-wave in the 12-lead ECG, or T-wave alternans (TWA) are associated with increased risk of sudden cardiac death[28-29]. Their detection with ECGI may be useful in predicting sudden cardiac death risk. The reproducibility of repolarization maps on a beat-to-beat basis when alternans are not present is also important, to demonstrate that these are not an artefact of the ECGI reconstruction.

The beat-to-beat variability of ECGI reconstructions was assessed using ECGI electrograms reconstructed using the method of fundamental solutions (MFS)[23] with zero-order Tikhonov regularization[25] and the CRESO method[27] to define the regularization parameter. Differences between successive T-waves was assessed using the CC, and the difference in amplitude of the T-waves. Differences between successive repolarization maps was assessed using CC and the AE. The median of each metric over 10 beats was computed.

For recorded electrograms, T-wave morphologies and repolarization maps were consistent and stable on a beat-to-beat basis for all experiments and electrodes indicating T-wave alternans were not present (summary of metrics in Figure S3). For ECGI, in all but one experiment for one drug setting, T-wave morphologies and repolarization maps were also consistent and stable. However, reconstructions were less stable than directly recorded maps.

Figure S4 presents reconstructed electrograms for the one exception where T-wave alternans were seen with ECGI. For this case, no alternans were present in recorded electrograms, nor visible from torso ECG. Further analysis showed the alternans in ECGI arose as the computed lambda value chosen for regularization also changed on a beat-to-beat basis. By fixing the lambda value to a constant, alternans were no longer present. We therefore advice verifying the lambda value is not a factor when alternans are present in ECGI reconstructions.

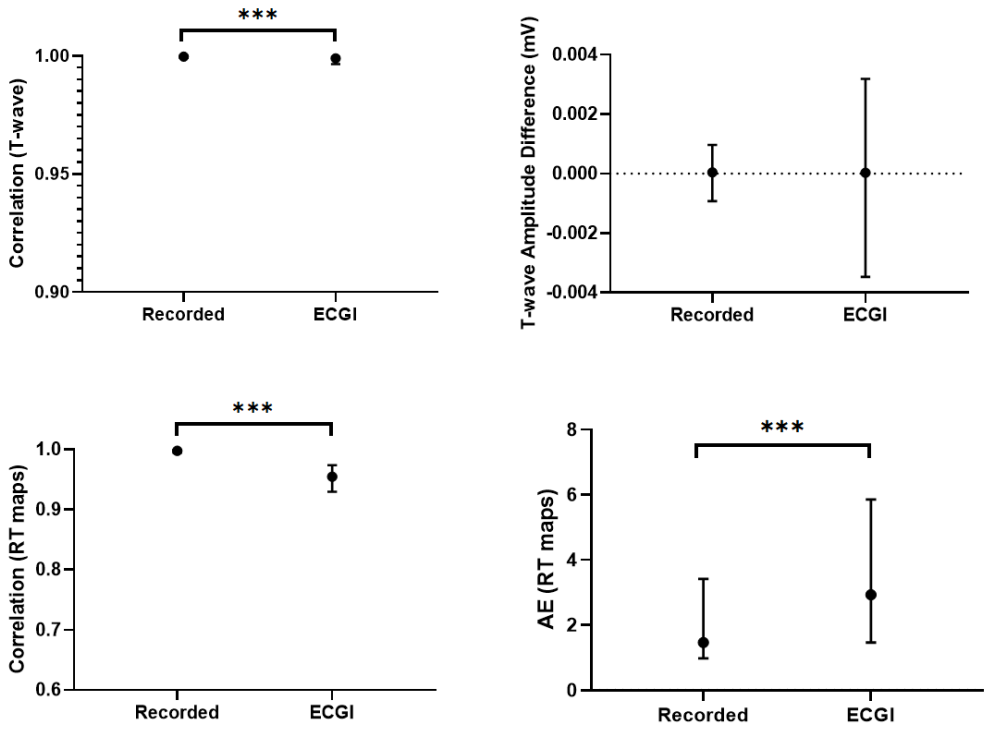

Figure S3.1: *Median beat-to-beat correlation of the T-waves (left top), amplitude difference in T-waves (right top), correlation of RT maps (left bottom) and AE of RT maps (right bottom) for recorded and ECGI reconstructed electrograms presented as median and interquartile ranges. Probabilities that distributions are significantly different: *** p≤0.0001.*

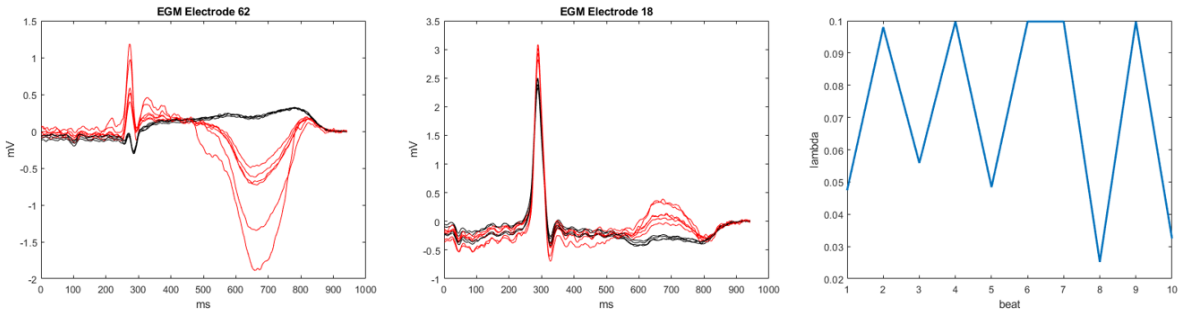

Figure S3.4: *Example ECGI reconstructed electrograms for the one case demonstrating T-wave alternans (left and middle) with computed lambda values for each beat (right). Electrograms in red were reconstructed with lambda < 0.07 and those in black with lambda > 0.07. No alternans were present in recorded electrograms, nor visible from torso ECG.*

S4. Regions of Early/Late Recovery

Though there was high qualitative consistency between the early and late repolarization regions of the heart in each study, the regions of early and late recovery appeared to be over- or under-estimated in size. Regions of abnormal recovery were defined as the electrodes with repolarization times outside the normal range, as defined from sock recordings in control state (no drugs) for each heart. The abnormally early and late regions defined by ECGI and sock recordings were compared in terms of the mean time in the region, and the size of the abnormal region (Figure S4.1). For each metric, the significance of differences was tested using paired t-tests with $p < 0.05$ defined as significant.

In the presence or absence of abnormally recovery regions, the timing of the early regions were accurately captured ($p = 0.95$, though the late regions repolarized 2.8 ± 0.7 ms earlier than recorded ($p<0.001$). However, ECGI significantly overestimated the size of the early regions by 11 ± 4 cm^2 ($p = 0.02$) and underestimated the size of late regions by 13 ± 3 mm^2 ($p < 0.0001$).

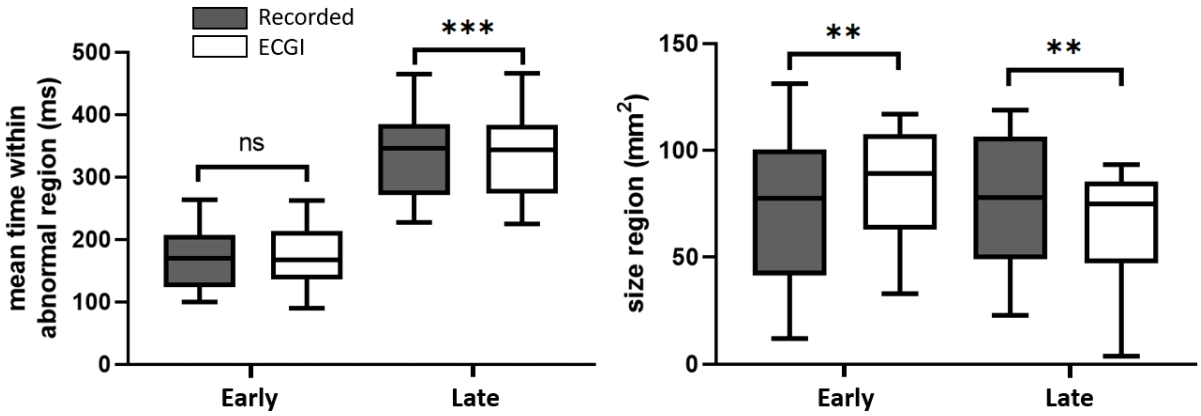

Figure S4.1: *Comparison of regions identified as abnormally early or late repolarizing using sock recordings and ECGI. Regions were compared in terms of mean time (ms) and area (mm^2).*

S5. Human Donor Heart

Recorded activation and RT maps for the human donor heart (Figure S5.1) demonstrated a suspected left bundle branch block, with early activation and repolarization on the RV, and late repolarization on the LV. Dofetilide and pinacidil perfusion created regions of late and early repolarization in non-LAD

and LAD (black dashed line) perfusion beds respectively. ECGI RT maps corresponded well to those recorded both at baseline and during drug perfusion. ECGI reconstructed T-waves (CC of 0.85 [0.52; 0.96]) and RT maps (CC = 0.69 [0.55; 0.77] and MAE = 31 [26; 52] ms) well, with no significant difference in CC or MAE values compared to those obtained in pig hearts (p = 0.07, 0.96 and 0.38 respectively)

ΔRT maps showed there was no strong gradients at baseline in either recorded or ECGI maps. With drug perfusion, a strong gradient developed at the border of the LAD perfusion bed in both recorded and ECGI maps.

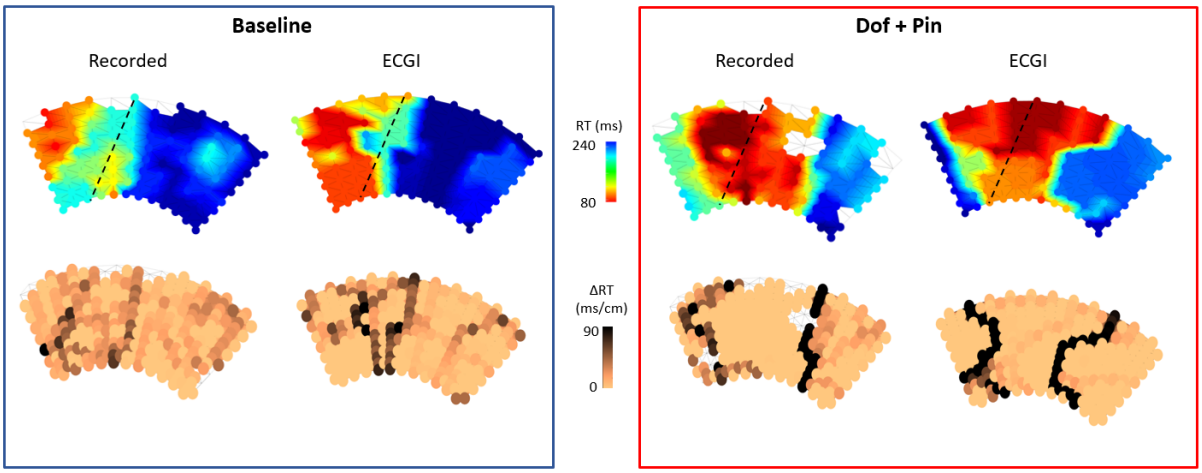

Figure S5. *Recorded and ECGI reconstructed RT maps (top) and ΔRT maps for the human donor heart at baseline (left) and during dofetilide and pinacidil perfusion through non-LAD and LAD (black dashed line) arteries respectively.*